Bioorganic & Medicinal Chemistry Letters 20 (2010) 4870–4877

Contents lists available at ScienceDirect

Bioorganic & Medicinal Chemistry Letters

journal homepage: www.elsevier.com/locate/bmcl

# 3-D-QSAR and docking studies on the neuronal choline transporter

Werner J. Geldenhuys [a,*], David D. Allen [a], Paul R. Lockman [b]

[a] Department of Pharmaceutical Sciences, Northeastern Ohio Universities Colleges of Medicine and Pharmacy, Rootstown, OH 44272, USA
[b] Department of Pharmaceutical Sciences, Texas Tech Health Sciences Center, School of Pharmacy, Amarillo, TX 79106, USA

ARTICLE INFO

*Article history:*
Received 5 May 2010
Revised 14 June 2010
Accepted 15 June 2010
Available online 26 June 2010

*Keywords:*
Membrane transporter
Organic cation transporter
Quantitative structure–property relationships
Nutrient transporter

ABSTRACT

The high affinity neuronal choline transporter (CHT1) is responsible for the uptake of choline into the pre-synaptic terminal of cholinergic neurons. Considering our past experience with modeling the blood–brain barrier choline transporter (BBBCHT) as drug delivery vector to the CNS, we investigated the 3-D-quantitative structure–activity relationship of the neuronal choline transporter. Comparative molecular field analysis (CoMFA) and comparative similarity index analysis (CoMSIA) yielded cross-validated models with a $q^2$ of 0.5, and a non-cross validated $r^2$ of 0.8. The electrostatic results of the 3-D-QSAR models are corroborated with a docking study into the bacterial choline transporter. Using this electrostatic map, we propose a putative binding site in a homology model of the CHT1. Knowledge gained from this study is useful to better understand the CHT1 as well as can be used in medicinal chemistry programs targeting this transporter.



Choline plays an important role in the bio-synthesis of the neurotransmitter acetylcholine. In the cholinergic nerve terminal, choline is taken up into the pre-synaptic terminal via one of two choline transporters. A low-affinity choline transporter which is generally involved in sequestering choline that is earmarked for processes such as membrane phospholipid synthesis as well as signaling lipids.[1–3] For the synthesis of the cholinergic system neurotransmitter, acetylcholine, the precursor choline is taken up into the terminal via a high affinity choline transporter (CHT1).[4,5] Two main characteristics separate the low and high affinity choline transporters; CHT1 uses a sodium dependent mechanism for transport, and CHT1 binds with high affinity ($K_i$ of 10–100 nM) by hemicholinium-3 (HC3).[6]

Importantly the uptake of choline through CHT1 is the rate limiting step in the synthesis of the neurotransmitter acetylcholine which plays a vital role in cognition. Recent literature has shown that CHT1 is downregulated in the age-related neurodegenerative disorder Alzheimer's disease.[7,8] Exploitation of this transporter by acetylcholine precursors may be of significant adjunctive benefit in the pharmacology of choline-esterase inhibitors (e.g., ladostigil, rivastimine) as a means to further increase the levels of acetylcholine in the brain.[9,10] Therefore a better understanding of the CHT1 is needed, and how the quaternary ammonium compound choline is selectively transported and if it can be exploited as a drug target.[2]

Recently, the group of Okuda et al. cloned CHT1 and interestingly, CHT1 shares sequence homology with sodium-glucose transproters.[6] However, the CHT1 crystal structure has not been resolved.[11] Previously, we have investigated the quantitative structure–activity relationships (QSAR) of quaternary ammonium compounds such as choline with affinity for the blood–brain barrier choline transporter (BBBCHT).[12–15] The BBBCHT plays an important role in sequestering choline from the plasma to the brain, since the BBB is essentially impermeable to charged compounds. Of interest is that CHT1 and BBCHT behave kinetically as two different transporters despite having significant overlap in there ability to bind cationic molecules.[16,17]

Given that the CHT1 may be a significant drug target for the Alzheimer's population, we have completed this work to gain a

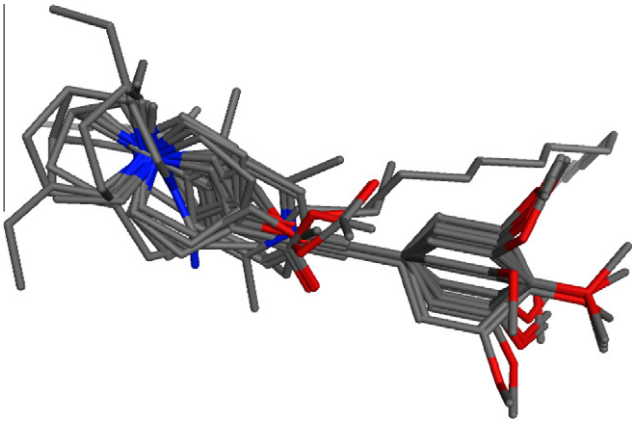

**Figure 1.** Alignment of the compounds used in this study.

* Corresponding author. Address: 4209, State Route 44, Rootstown, OH 44272, USA. Tel.: +1 330 325 6474; fax: +1 330 325 5936.
*E-mail address:* wgeldenh@neoucom.edu (W.J. Geldenhuys).

0960-894X/$ - see front matter © 2010 Elsevier Ltd. All rights reserved.
doi:10.1016/j.bmcl.2010.06.090

**Table 1**
Structures of the quaternary ammonium compounds used for the 3-D-QSAR study[20]

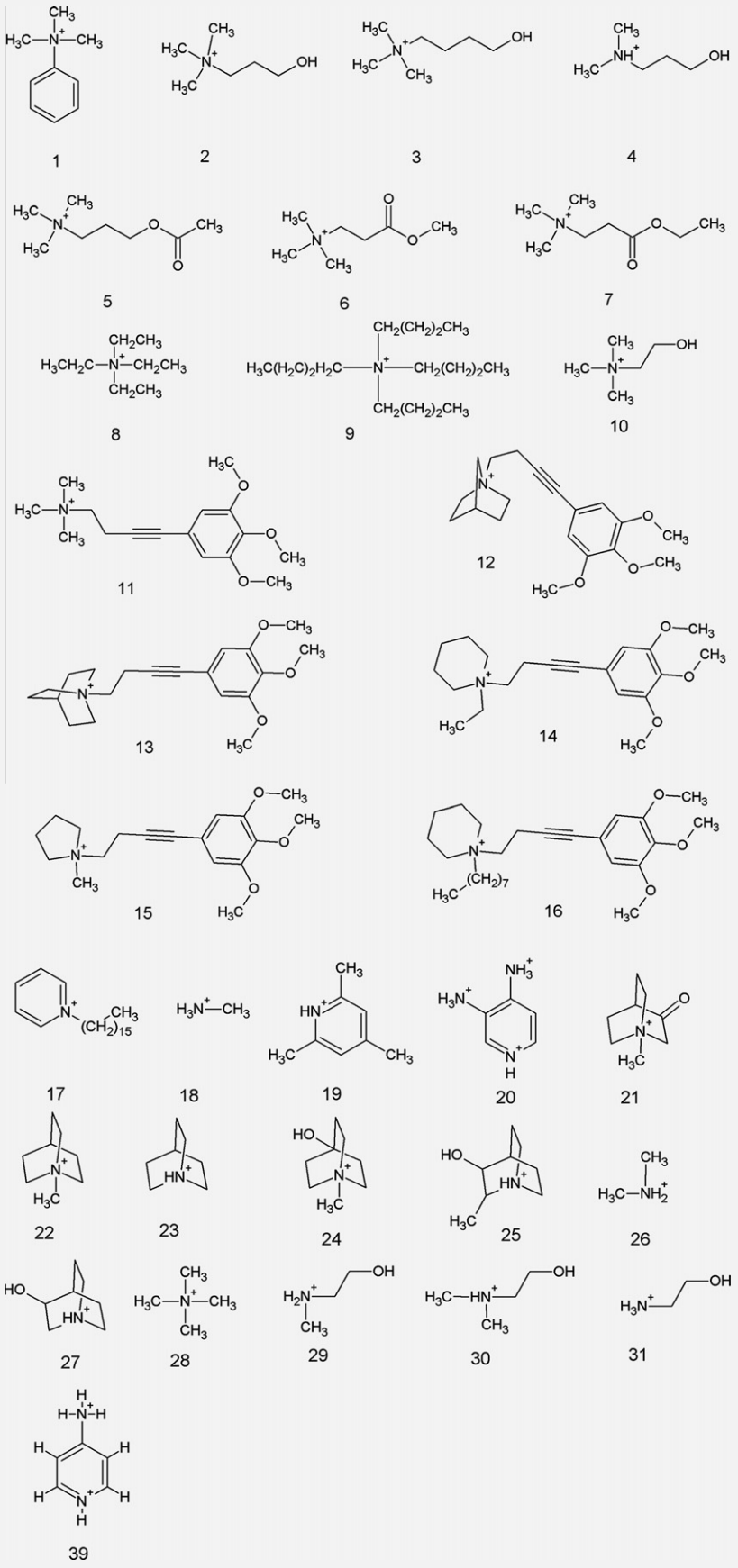


(*continued on next page*)

**Table 1** *(Continued)*

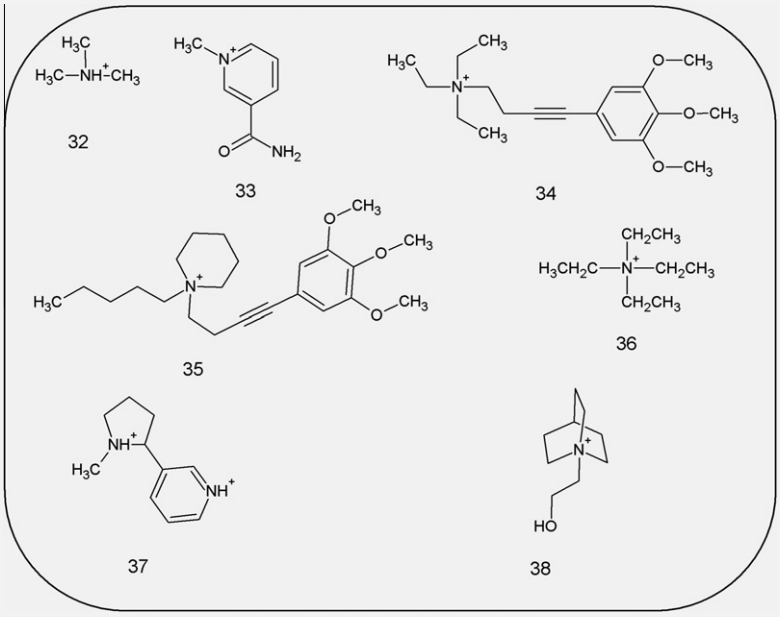


Compounds shown circled constitute the test set used.

clearer understanding of the structure–activity relationships of the CHT1. Here we present for the first time a 3-D-QSAR study of the CHT1.

3-D-QSAR modeling was done using the QSAR module of SYBYL-X (Tripos, St Louis MO). Compound alignment for CoMFA and CoMSIA models were performed using the software suite from Openeye (Santa Fe, NM, USA). Compounds (Table 1) were drawn in MarvinSketch vs. 5.2 (www.chemaxon.com) which was then used for the alignment of the compounds (Fig. 1). OMEGA (Openeye) is a conformer generating program, which was used to generate multiple conformers of each compound.[18] ROCS 3.0 (Openeye) was used for the alignment of the compounds by using the conformer library of compounds generated by OMEGA, so that both shape overlay and chemical (color) overlay was used, with choline as the query structure.[19] Initial inspection of the results from the ROCS overlay, showed that three compounds, which contained the 3,4,5-trimethoxy-sutbstitution were at first superimposed with the cationic nitrogen opposite of that of choline, probably due to favoring of molecular structure and conformation over electrostatics. The resulting overlay of compounds (Fig. 1) was then used for the CoMFA and CoMSIA analyses. The compounds used to develop the models were divided into a training set (1–30, 39) and a test set (32–38) using the QSAR Wizard program for MOE which is available for download at the Chemical Computing group SVL exchange (http://svl.chemcomp.com/). The complete set was randomly divided irrespective of activity or chemical composition, so that an 80% separation could be achieved.

Gasteiger–Hückel charges were added before the CoMFA calculation. Default values provided in the Tripos CoMFA module were used with a 2.0 Å grid spacing using a $sp^3$ carbon atom with a +1 point charge as a probe to explore the steric and electrostatic interactions at the lattice points in the grid. The default cut-off value was set at 30 kcal/mol. Statistical analysis was performed

**Table 2**
Results from the 3-D-QSAR analysis

| | CoMFA | CoMSIA |
|---|---|---|
| *Cross-validated* | | |
| $q^2$ | 0.504 | 0.558 |
| SEP | 1.095 | 1.114 |
| Number of components | 3 | 4 |
| *Non-cross validated* | | |
| $r^2$ | 0.815 | 0.895 |
| SEE | 0.692 | 0.549 |
| *F* | 39.679 | 40.715 |
| Steric | 0.884 | 0.541 |
| Electrostatic | 0.116 | 0.459 |

Abbreviations are: standard error of prediction (SEP); standard error of estimate (SEE).

**Table 3**
Predicted affinities for the CoMFA and CoMSIA training set

| | $pK_i$ | COMFA_PRED | Residual | CoMSIA | Residual |
|---|---|---|---|---|---|
| **1** | 4.124 | 4.03 | −0.094 | 3.631 | −0.493 |
| **2** | 5.657 | 4.618 | −1.039 | 4.942 | −0.715 |
| **3** | 3.508 | 4.709 | 1.201 | 4.732 | 1.224 |
| **4** | 3.537 | 4.454 | 0.917 | 3.893 | 0.356 |
| **5** | 3.721 | 3.93 | 0.209 | 3.669 | −0.052 |
| **6** | 3.5686 | 4.052 | 0.4834 | 3.497 | −0.0716 |
| **7** | 3.4685 | 3.991 | 0.5225 | 3.411 | −0.0575 |
| **8** | 4.619 | 4.737 | 0.118 | 5.037 | 0.418 |
| **9** | 2.978 | 2.875 | −0.103 | 2.683 | −0.295 |
| **10** | 6.167 | 4.692 | −1.475 | 5.083 | −1.084 |
| **11** | 5.6989 | 6.318 | 0.6191 | 5.733 | 0.0341 |
| **12** | 7.301 | 7.289 | −0.012 | 7.492 | 0.191 |
| **13** | 7.0457 | 6.932 | −0.1137 | 6.963 | −0.0827 |
| **14** | 6.744 | 6.662 | −0.082 | 6.617 | −0.127 |
| **15** | 6.698 | 6.886 | 0.188 | 6.701 | 0.003 |
| **16** | 6.638 | 6.304 | −0.334 | 6.873 | 0.235 |
| **17** | 4.494 | 3.623 | −0.871 | 4.319 | −0.175 |
| **18** | 1.455 | 1.887 | 0.432 | 1.582 | 0.127 |
| **19** | 3.97 | 2.571 | −1.399 | 3.609 | −0.361 |
| **20** | 3.086 | 2.933 | −0.153 | 3.188 | 0.102 |
| **21** | 6.283 | 5.284 | −0.999 | 5.902 | −0.381 |
| **22** | 5.3279 | 4.854 | −0.4739 | 4.804 | −0.5239 |
| **23** | 4.397 | 4.15 | −0.247 | 3.946 | −0.451 |
| **24** | 4.142 | 4.823 | 0.681 | 5.358 | 1.216 |
| **25** | 3.677 | 4.276 | 0.599 | 3.871 | 0.194 |
| **26** | 2.026 | 2.348 | 0.322 | 2.476 | 0.45 |
| **27** | 3.677 | 4.36 | 0.683 | 4.018 | 0.341 |
| **28** | 4.522 | 4.192 | −0.33 | 4.462 | −0.06 |
| **29** | 2.42 | 3.168 | 0.748 | 3.009 | 0.589 |
| **30** | 4.254 | 4.213 | −0.041 | 3.706 | −0.548 |
| **39** | 3.318 | 3.362 | 0.044 | — | — |

**Table 4**
Predicted affinities for the CoMFA and CoMSIA test sets

| | $pK_i$ | CoMFA | Residuals | CoMSIA | Residuals |
|---|---|---|---|---|---|
| **31** | 0.8239 | 2.6608 | 1.8369 | 2.187886 | 1.363986 |
| **32** | 3.4685 | 3.188 | −0.2805 | 3.3406 | −0.1279 |
| **33** | 3.443 | 2.927 | −0.516 | 3.8817 | 0.4387 |
| **34** | 6.154 | 6.393 | 0.239 | 6.1985 | 0.0445 |
| **35** | 7.698 | 6.413 | −1.285 | 6.4132 | −1.2848 |
| **36** | 3.585 | 3.662 | 0.077 | 3.78215 | 0.19715 |
| **37** | 3.2839 | 4.797 | 1.5131 | 3.20319 | −0.08071 |
| **38** | 6.1938 | 5.069 | −1.1248 | 5.93725 | −0.25655 |

using the partial least squares method (PLS) implemented in the SYBYL program. Non-cross validated ($r^2$) values were determined for the models using linear regression analysis (with variances reported as the standard error of estimation, SEE) which are considered significant when $r^2$ is greater than 0.7. The $q^2$ values obtained were considered significant at 0.3. The 3-D graphical representation of the steric and electrostatic fields generated through CoMFA and CoMSIA are shown with the relative contributions represented as a 3-D coefficient map with favored 80% steric (green) and electrostatic (blue) effects and 20% disfavored steric (yellow) and electrostatic effects (red). Green colored areas of the map indicate where steric bulky groups may enhance interaction affinity. Blue colored areas (80%) indicate regions where a more positively charged group will likely lead to increased binding affinity, while red areas indicate where a more negatively charged group will likely lead to increased binding (20%). Biological data are from the literature[20] and entered as $pK_i$ values in the spreadsheets accessed by the CoMFA routine in SYBYL (Tables 2 and 3).

The results from the CoMFA analysis are given in Table 2. As can be seen the cross-validated PLS $r^2$ ($q^2$) was found to be 0.5, suggesting that the CoMFA model is statistically significant where models with $q^2$ >0.3 are generally considered to be able to be predictive in nature. The optimum number of components from the PLS was seen to be 3. The non-cross validated regression gave an $r^2$ of 0.818, suggesting that the model would be able to predict the activity of a compound 81% of the time. The contributions from the steric and electrostatic fields were seen to be 88% and 11%, respectively. This was surprising since the compounds used to develop the CoMFA model are all cationic charged compounds. The large contribution from the steric fields suggested a probable volume restrictions based in the neuronal choline transporter. Since a CoMFA model needs to be validated by an test set, we also predicted the affinity for the neuronal choline transporter for a test set of eight compounds (Table 4). As shown in Figure 2A and Table 2, the CoMFA model was able to predict the affinity of the compounds with an $r^2$ of 0.769, suggesting that the CoMFA model is able to accurately predict the affinity of compounds of ~77%. Inspection of the residuals indicated compounds **37** and **31** were not well predicted by the model.

Figure 2B shows the steric and electrostatic CoMFA maps. The green steric maps show areas where increasing bulk would likely lead to an increase in activity, while yellow steric maps indicate areas where they would lead to a decrease in activity. Choline is shown in Figure 2B with the steric and electrostatic maps. We observed that there exists a zone of optimal steric favor surrounding the cationic nitrogen. This 'optimum' area indicates why choline (**10**) would have a high affinity for the neuronal choline transporter, as compared to compounds such as **4**, **29**, and **30**. In addition, there is a steric restrictive (yellow) site located close to the hydroxyl moiety of choline. Blue electrostatic maps indicate areas where positive charge would likely lead to an increase in activity, whereas red maps indicate areas where negative charge would likely lead to an increase in affinity. As expected, a large area surrounding the cationic nitrogen of choline is identified by the blue map. In addition, a relatively smaller red map is shown close to the hydroxyl moiety of choline. These maps indicate that the rela-

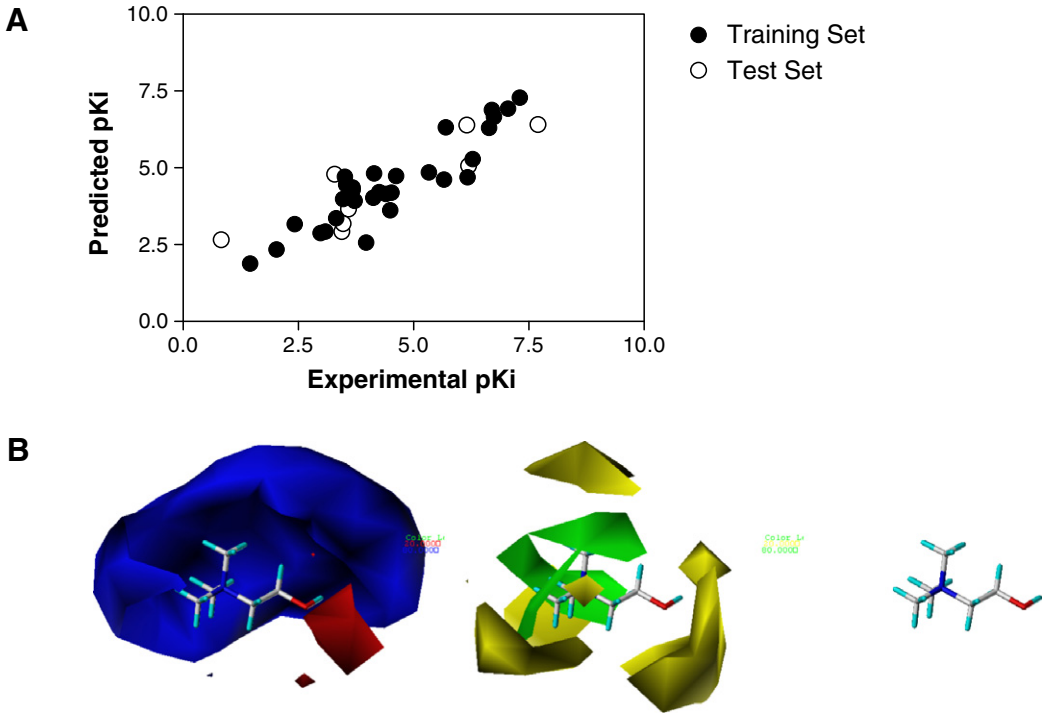


**Figure 2.** (A) CoMFA maps shown with choline as reference molecule. Steric maps are shown where green maps indicate areas where increasing the steric bulk of the compound will likely lead to an increase in activity, and yellow, where steric bulk is likely to lead to a decrease in activity. Electrostatic maps are shown where blue indicates areas where positive charges will likely lead to an increase in activity, while red areas will favor negative charges; (B) predicted $pK_i$ from the CoMFA training set model compared to the experimental $pK_i$ values.

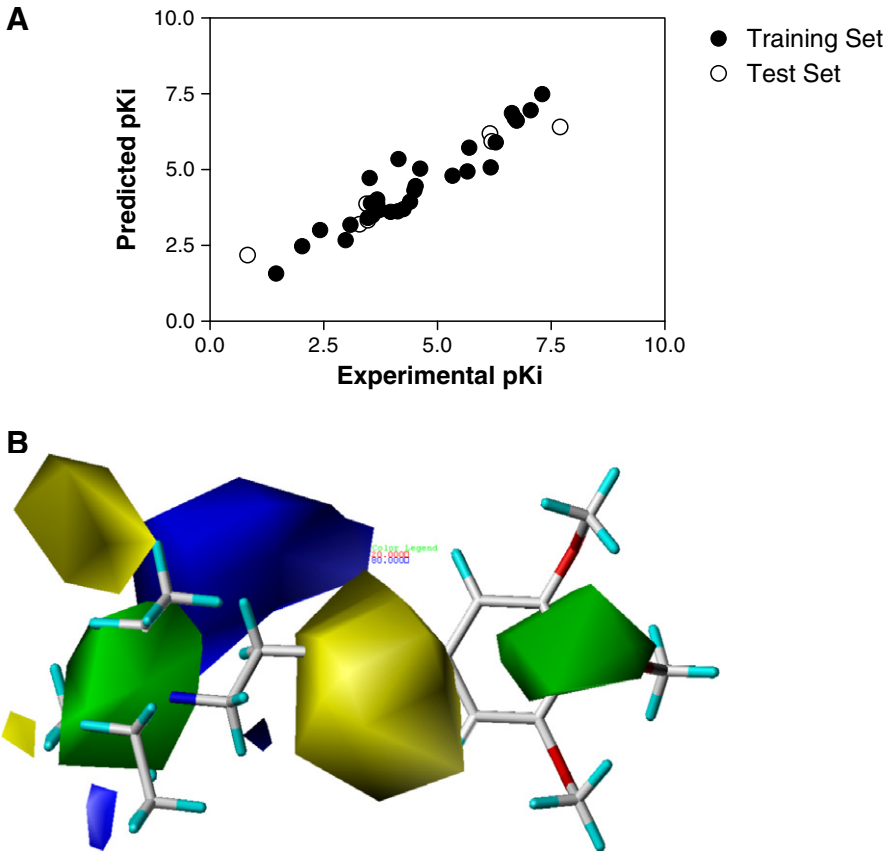


**Figure 3.** (A) CoMSIA maps shown with choline and a 3,4,5-trimethoxy-derivative as reference molecules. Steric maps are shown where green maps indicate areas where increasing the steric bulk of the compound will likely lead to an increase in activity, and yellow, where steric bulk is likely to lead to a decrease in activity. Electrostatic maps are shown where blue indicates areas where positive charges will likely lead to an increase in activity, while red areas will favor negative charges; (B) predicted p$K_i$ from the CoMSIA training set model compared to the experimental p$K_i$ values.

tive separation of positive and negative charge in choline is close to optimal for binding to the neuronal choline transporter, as would be expected for the physiological substrate.

The results from the CoMSIA analysis is shown in Table 2. As with the CoMFA model, we used steric and electrostatic fields in the CoMFA analysis. Initially, when we developed the CoMSIA models, only the steric fields would lead to a $q^2$ >0.3, while the electrostatic fields alone yielded a $q^2$ <0.3 (data not shown). We therefore combined the steric and electrostatic fields to be able to compare the CoMSIA model with the CoMFA model directly. Compound **39** was removed as outlier before building the final model. PLS cross-validation resulted in a regression value ($q^2$) of 0.554, suggesting a predictive model was obtained, as in the case of the CoMFA model. The optimum number of components found from the cross-validation was used to develop the non-cross validated regression model, which gave a $r^2$ of 0.895. The relative contributions of the steric and electrostatic fields were 54% for steric contribution and 46% for electrostatic contribution. To validate the CoMSIA model, we predicted the test set compounds' p$K_i$ values for the neuronal choline transporter. As can be seen from Figure 3A, the CoMSIA model which used steric and electrostatic fields was able to predict the p$K_i$ values for the test set with an $r^2$ of 0.94. Compared to the CoMFA model, the CoMSIA model appears to be more predictive in nature, potentially because of the treatment of the Lennard-Jones potentials which are not as sharp as in CoMFA, and that CoMSIA extracts more information regarding the compounds structurally.

The CoMSIA model is shown in Figure 3B with one of the 3,4,5-trimethoxy compounds shown. Green maps indicate areas where adding sterically bulky groups will likely lead to an increase in activity, while the yellow areas are disfavored for steric bulky groups. As can be seen from Figure 3B, there is a large green area surrounding the cationic nitrogen, which correlates with the findings of the CoMFA model, in that there is a limited increase in bulk which can be added to the cationic nitrogen to increase affinity, but similarly to the CoMFA model, this increase in steric bulk is restricted by an additional area outside of the green area where increase in bulk would decrease activity. Additionally, there is a yellow area spanning the position where choline's hydroxy-moiety would be located, and corresponds to the unsaturated bond of the 3,4,5-trimethoxy compounds.

Although CoMFA maps generally should not be used as 'pseudo-receptor maps', the distinct bands of sterically allowable and disallowable space may suggest that the yellow areas are the limit of the amino acids which surround the binding pocket. Similarly, the large positive blue map and small negative red map, may indicate that there may be a large electronegative area which accommodates the positive charge on the cationic nitrogen, and a single amino acid which allows for a hydrogen bond with the hydroxyl group on choline.

To date, no X-ray crystal structure has been published of the human neuronal choline transporter. To gain some insight into what the possible electrostatic character might be of such a 3-D choline transporter, we looked at the bacterial choline transporter with acetylcholine co-crystalized (2RIN.pdb).[21] As can be seen in Figure 4, we docked (using MOE-Dock) **10** (choline) (Fig. 4A and B), where Figure 4A shows the electrostatic surface maps of choline inside the binding pocket, and Figure 4B, the ligand interactions

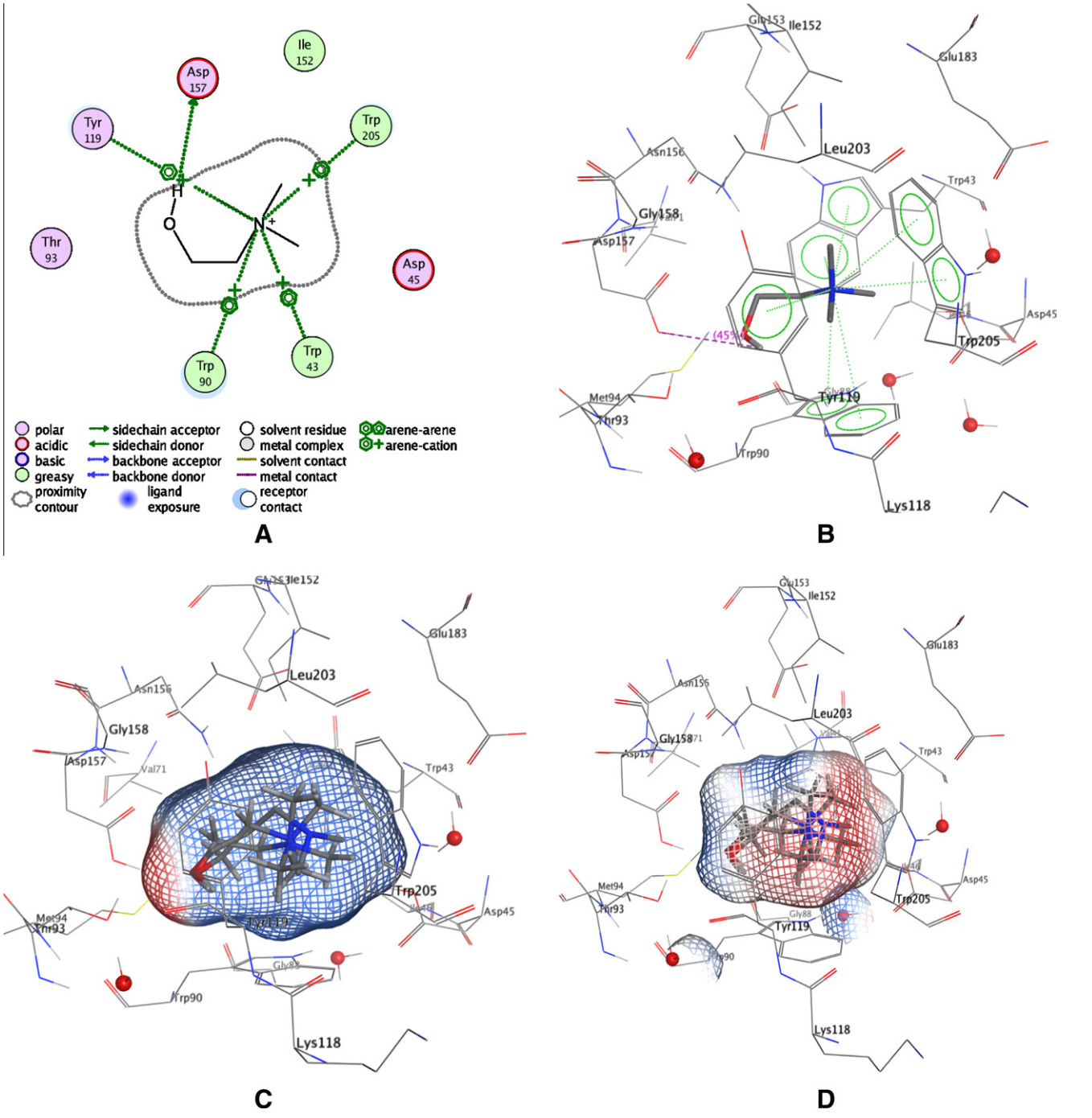


**Figure 4.** Docking of choline into the binding site of the bacterial choline transporter (2RIN).[21] (A) 2D interaction map showing important amino acids which play a role in binding; (B) docked pose of choline; (C) electrostatic map of **10**, **30**, and **4** docked into the binding site, showing positive surface charges as blue and negative charge distribution as red; (D) electrostatic map of the interior cavity of the binding pocket, showing positive surface charge distribution as blue and negative charge distribution as red.

with the animo acids of the binding site in a 2D representation. **30** and **4** were also docked into the binding pocket of the choline transporter, and are seen to fit well into the electrostatic map of the ligands (Fig. 4C), while we also show the electrostatic surface of the binding pocket (Fig. 4D) The bacterial choline transporter has three tryptophane amino acids, (TRP205, TRP90, and TRP43; Fig. 4A) which are all the aromatic rings that coordinate with the cationic nitrogen, and the ASP157 which is able to undergo a hydrogen bond with the hydroxyl group of choline and the derivatives docked. Evaluation of the electrostatic surface of the binding cavity, shows a large negative character near the tryptophanes, and a more positive character near the ASP157. These electrostatic fields (Fig. 4C) are inversely correlate when an electrostatic grid is drawn over the docked compounds (Fig. 4D), where the large positive space on the ligand generated map and the smaller negative ligand map, also corresponds well with the CoMFA maps. Using this electrostatic map as starting point, we can build a homology model of CHT1, with a sodium/galactose symporter (3dh4.pdb), using the A-chain,[22] by using the i-Tasser server (http://zhanglab.ccmb.med.umich.edu/I-TASSER/) and TCoffee for sequence align-

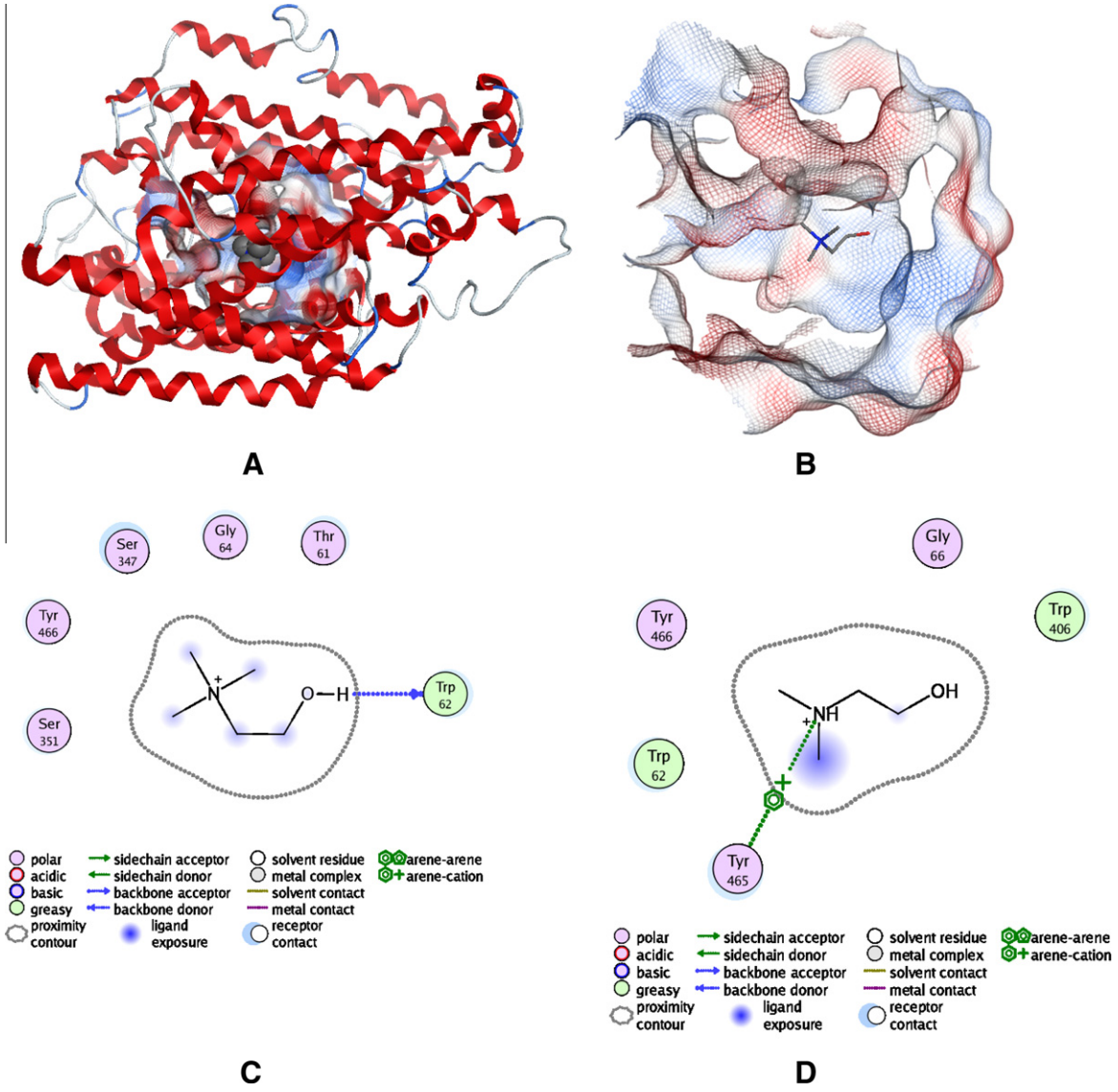


**Figure 5.** (A) Homology model of the neuronal choline transporter based on a sodium/glucose symporter, 3dh4.pdb; (B) electrostatic map of the proposed binding pocket, with positive areas shown in blue and negative areas shown in red; (C) ligand interaction diagram showing **10** docked; (D) ligand interaction diagram showing **4** docked.

ment (http://www.igs.cnrs-mrs.fr/Tcoffee/tcoffee_cgi/index.cgi) (see Supplementary data for alignment). To identify putative binding pockets, we used SiteFinder (MOE). By drawing electrostatic surface maps on the binding pocket identified by SiteFinder, we chose a putative binding site located near the middle of the transporter (Fig. 5A). As can be seen in Figure 5B, the electrostatic maps closely mimics the electrostatic surface characteristics of the bacterial choline transporter (refer to Fig. 4D). We docked choline into this putative site, which suggested a hydrogen bond with TRP62 (Fig. 5C). As expected, the weaker compound, **4**, which differs from choline by one methyl group, docked so that a weaker cation-aromatic bond is formed, as opposed to the stronger hydrogen bond between the hydroxyl group of choline and the transporter. This difference in binding agrees with the experimental affinity.

Previously, we developed a 3-D-QSAR of the BBBCHT,[12–15] which has been shown to behave kinetically different than CHT1.[16,17] When comparing the two 3-D-QSAR studies, similar 'gross' structural features are seen, although in the BBBCHT, the restriction in steric space surrounding the cationic nitrogen is more localized. Considering the physiological role of these transporters, that is, transport of choline, the tertiary protein structure may be very similar in nature, but it may be plausible that that the local environment, that is, the brain vasculature versus pre-synaptic neuronal membrane affects the kinetic nature of the protein and may restrict the closed substrate pocket size.

In conclusion, here we describe for the first time a 3-D-QSAR model for the neuronal choline transporter. Both the CoMFA and CoMSIA models were recently predictive as shown by use of a test set. The cationic nitrogen may have a limited scope where bulky groups will lead to increased activity, and similarly, the hydroxyl group indicates a point of hydrogen bonding, although other acceptor/donor sites are not excluded from this model. Results from this study could be used in the design of compounds which are targeted for use in diseases where choline and acetylcholine play an important role, as well as may be useful as a possible quantitative structure–property relationship filter for large virtual databases.

## Supplementary data

Supplementary data associated with this article can be found, in the online version, at doi:10.1016/j.bmcl.2010.06.090.

## References and notes


1. Canty, D. J.; Zeisel, S. H. *Nutr. Rev.* **1994**, *52*, 327.
2. Fujii, T.; Masai, M.; Misawa, H.; Okuda, T.; Takada-Takatori, Y.; Moriwaki, Y.; Haga, T.; Kawashima, K. *J. Neurosci. Res.* **2009**, *87*, 3024.
3. Okuda, T.; Haga, T. *Neurochem. Res.* **2003**, *28*, 483.
4. Haga, T.; Noda, H. *Biochim. Biophys. Acta* **1973**, *291*, 564.
5. Yamamura, H. I.; Snyder, S. H. *Science* **1972**, *178*, 626.
6. Okuda, T.; Haga, T.; Kanai, Y.; Endou, H.; Ishihara, T.; Katsura, I. *Nat. Neurosci.* **2000**, *3*, 120.
7. Rodriguez-Puertas, R.; Pazos, A.; Zarranz, J. J.; Pascual, J. *J. Neural Transm. Park. Dis. Dement. Sect.* **1994**, *8*, 161.
8. Pascual, J.; Fontan, A.; Zarranz, J. J.; Berciano, J.; Florez, J.; Pazos, A. *Brain Res.* **1991**, *552*, 170.
9. Birks, J. *Cochrane Database Syst. Rev.* **2006**, CD005593.
10. Lam, B.; Hollingdrake, E.; Kennedy, J. L.; Black, S. E.; Masellis, M. *Hum. Genomics* **2009**, *4*, 91.
11. Chang, C.; Ray, A.; Swaan, P. *Drug Discovery Today* **2005**, *10*, 663.
12. Geldenhuys, W. J.; Manda, V. K.; Mittapalli, R. K.; Van der Schyf, C. J.; Crooks, P. A.; Dwoskin, L. P.; Allen, D. D.; Lockman, P. R. *Bioorg. Med. Chem. Lett.* **2010**, *20*, 870.
13. Geldenhuys, W. J.; Lockman, P. R.; Nguyen, T. H.; Van der Schyf, C. J.; Crooks, P. A.; Dwoskin, L. P.; Allen, D. D. *Bioorg. Med. Chem.* **2005**, *13*, 4253.
14. Lockman, P. R.; McAfee, J. H.; Geldenhuys, W. J.; Allen, D. D. *Neurochem. Res.* **2004**, *29*, 2245.
15. Geldenhuys, W. J.; Lockman, P. R.; McAfee, J. H.; Fitzpatrick, K. T.; Van der Schyf, C. J.; Allen, D. D. *Bioorg. Med. Chem. Lett.* **2004**, *14*, 3085.
16. Allen, D. D.; Lockman, P. R. *Life Sci.* **2003**, *73*, 1609.
17. Lockman, P. R.; Allen, D. D. *Drug Dev. Ind. Pharm.* **2002**, *28*, 749.
18. Hawkins, P. C.; Skillman, A. G.; Warren, G. L.; Ellingson, B. A.; Stahl, M. T. *J. Chem. Inf. Model.* **2010**, *50*, 572.
19. Hawkins, P. C.; Skillman, A. G.; Nicholls, A. *J. Med. Chem.* **2007**, *50*, 74.
20. Tamaru, M.; Roberts, E. *Brain Res.* **1988**, *473*, 205.
21. Oswald, C.; Smits, S. H.; Hoing, M.; Sohn-Bosser, L.; Dupont, L.; Le Rudulier, D.; Schmitt, L.; Bremer, E. *J. Biol. Chem.* **2008**, *283*, 32848.
22. Faham, S.; Watanabe, A.; Besserer, G. M.; Cascio, D.; Specht, A.; Hirayama, B. A.; Wright, E. M.; Abramson, J. *Science* **2008**, *321*, 810.